Image Quality Analysis of Limited Angle Tomography Using the Shift-Variant Data Loss Model

Yixing Huang[1], Guenter Lauritsch[2], Mario Amrehn[1], Oliver Taubmann[1], Viktor Haase[3], Daniel Stromer[1], Xiaolin Huang[1], Andreas Maier[1]

[1]Pattern Recognition Lab, Friedrich-Alexander-University Erlangen-Nuremberg
[2]Siemens Healthcare GmbH, Forchheim
[3]Institute for Signal Processing, University of Lübeck
yixing.yh.huang@fau.de

Abstract. This paper investigates the application of the shift-variant data loss (SVDL) model in image quality assessment for a state-of-the-art reconstruction technique, the weighted total variation (wTV), in limited angle tomography. The SVDL model is used to analyze the acquired frequency information in 2-D fan-beam limited angle tomography. The wTV algorithm is applied to reconstruct some specific mathematical phantoms. The experiments show that the reconstructed image quality depends on the relation of the source trajectory and geometric structure of the imaged object, position, shape, size and orientation in particular.

1 Introduction

Constraints arising from the practical design of X-ray imaging devices used in computed tomography (CT) reconstruction may sometimes limit their gantry rotation such that not all required angles can be acquired. In limited angle tomography, some information is lost and streak artifacts occur due to the data loss. Steven et al. [1] proposed a shift-variant data loss (SVDL) model using local Fourier transforms to analyze the data loss in cone-beam CT with a circular trajectory. Similarly, it can also be applied to limited angle tomography.

The data loss makes compressed sensing (CS) technologies, especially total variation (TV) algorithms, more attractive because CS can use relatively few data retaining a good reconstruction result. Recently, a variety of TV algorithms such as iTV [2], ASD-POCS+TV [3], anisotropic TV [4], and spatial-temporal TV regularization (STTVR) [5] have been developed. Pan et al. [6] demonstrated that iterative reconstruction methods with TV minimization can reduce streak artifacts well in limited angle tomography. However, the staircasing effect may blur the reconstructed image. In 2008, Candès et al. [7] proposed the weighted total variation (wTV) algorithm to enhance sparsity, which can avoid staircasing effects and preserve the sharp edges better than the non-weighted TV algorithm.

In this paper, we use the SVDL model to analyze the acquired frequency information in fan-beam limited angle tomography and investigate the quality of images reconstructed with the wTV algorithm.

2 Materials and Methods

2.1 The Shift-variant Data Loss Model

In 2-D fan beam CT, a $\pi + 2\gamma_{\max}$ short scan is sufficient and necessary for reconstruction, where $\gamma_{\max}$ is half a fan angle. However, in limited angle tomography, the scan angle is less than that. Thus, some information of the object is not acquired and streak artifacts occur due to the data loss. Here we use a fan-beam geometry with $\beta_{\min} = 0°$, $\beta_{\max} = 160°$, $\gamma_{\max} = 10°$ and $d = 2175$ mm to describe the SVDL model, where $\beta_{\min}$ and $\beta_{\max}$ are the start and end source rotation angle and d is the source to detector distance. The trajectory is shown in Fig. 1.

The SVDL model describes the data loss in frequency domain. In Fig. 1, only the local small neighborhood of the point $\mathbf{x} = (x, y)$ is considered. Rays intersecting this neighborhood can be regarded as parallel rays since the X-ray source is far away in comparison. Thus, the central slice theorem known for parallel-beam geometry can be applied here to analyze the data loss in the frequency domain. When the source is at the start position S_0 ($\beta = \beta_{\min}$), according to the central slice theorem, the red line, which is perpendicular to the ray from S_0 to $\mathbf{x}$ and forms the angle η_1 with the Y-axis, is measured in the frequency domain. Similarly, when the source is at the end position S_1 ($\beta = \beta_{\max}$), the red line with the angle η_2 is measured. Therefore, the sector between the angles η_1 and η_2 is acquired and a double wedge area (shaded area) is lost. The two boundary angles for the double wedge can be calculated as

$$\eta_1 = \operatorname{atan}\left(\frac{y + D\sin\beta_{\min}}{D\cos\beta_{\min} - x}\right), \qquad \eta_2 = \operatorname{atan}\left(\frac{x - D\cos\beta_{\max}}{y + D\sin\beta_{\max}}\right) + \frac{\pi}{2} \tag{1}$$

2.2 Iterative Reweighted Total Variation Algorithm

The objective function using wTV minimization for limited angle reconstruction is

$$\min_{\boldsymbol{f}} ||\boldsymbol{f}||_{\mathrm{wTV}} \quad \text{subject to} \quad ||\boldsymbol{A}\boldsymbol{f} - \boldsymbol{p}||_2^2 \leq \varepsilon \tag{2}$$

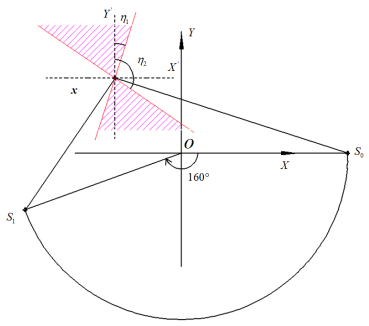

Fig. 1. The scan trajectory and a sketch of the shift-variant data loss model. The X-ray source rotates from S_0 ($\beta = 0°$) to S_1 ($\beta = 160°$). The red lines with angles η_1 and η_2 are the minimum and maximum frequency components available in frequency domain, respectively. The shaded area shows the region where data is missing (double wedge shape).

where $\boldsymbol{f}$ is the image, $\boldsymbol{A}$ is the system projection matrix, $\boldsymbol{p}$ is the acquired projection data and ε is a small value for the data consistency error. Based on Candés' wTV algorithm [7], $||\boldsymbol{f}||_{\mathrm{wTV}}$ is defined as:

$$||\boldsymbol{f}||_{\mathrm{wTV}} = \sum_{i,j} \boldsymbol{W}_{i,j} || \left(\mathcal{D}\boldsymbol{f}\right)_{i,j} ||_2 \qquad \text{where } \boldsymbol{W}_{i,j} = \frac{1}{||(\mathcal{D}\boldsymbol{f})_{i,j}||_2 + \epsilon} \tag{3}$$

$\boldsymbol{W}$ is the weight matrix, i and j are pixel indices, $\mathcal{D}\boldsymbol{f}$ is the gradient of the image $\boldsymbol{f}$ and ϵ is a parameter that influences the reconstruction convergence speed and reconstructed image resolution.

All images are reconstructed with $\epsilon = 0.001$ in Eqn. (3) chosen heuristically and the reconstruction results are obtained when the algorithm reaches the termination criterion $r < 1.0^{-7}$, where r is the root-mean-square difference of two iteration results.

2.3 Simulated Phantom Design

To investigate the relation between the SVDL model and the image quality reconstructed with the wTV algorithm, three groups of phantoms are designed. The detector size is 768 pixels and the pixel size is 1 mm. The angular increment is 1°, $\gamma_{\max} = 10°$ and $d = 2175$ mm. The whole experimental setup, including generation of the phantoms, was implemented in CONRAD [8].

The first phantom (Fig. 2(a)) is a mix of circular areas and lines. The image size is 512×512, the radii for the outer and inner boundary circles are 230 and 205 pixels respectively. The widths of the four lines and the radii of the eight small circular areas are both 3 pixels. The lines and the small circles are located at different positions. The attenuation coefficients for the white and black areas are 1/pixel and 0 respectively. The attenuation coefficient for the small circular areas and the lines is 0.7/pixel, and for the area between the two large circles it is 0.4/pixel.

The second group consists of two phantoms, shown on the left of Fig. 3. The rectangles in each phantom have the same width but different lengths. The sizes are 50×5 and 150×5 respectively and the distance between two rectangles is 5 pixels. For the first phantom and second group of phantoms, $(\beta_{\min}, \beta_{\max}) = (0°, 160°)$.

The third phantom shown in Fig. 4(a) also consists of rectangles but with the size 80×5. In order to get different phantom orientations relative to the source trajectory, three scan trajectories are adopted. The scan trajectories are $(\beta_{\min}, \beta_{\max}) = (-10°, 150°)$, $(0°, 160°)$ and $(10°, 170°)$.

3 Results

3.1 Shape and Position Dependency

In Fig. 2, the wTV reconstruction result (Fig. 2(d)) shows that the line structure at the top position is missing while all other structures are reconstructed very

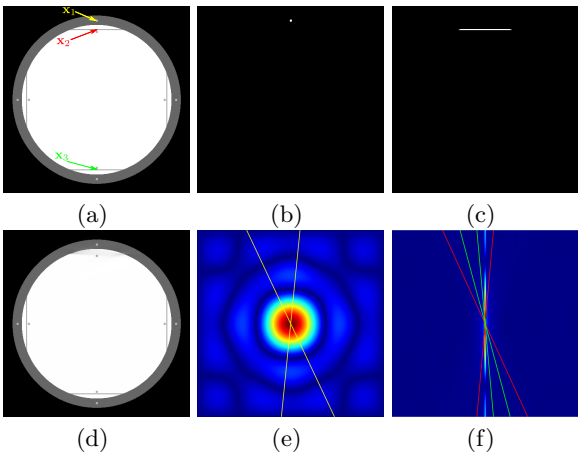

Fig. 2. (a) Phantom. (b) Top circular area. (c) Top line. (d) Reconstruction. (e) Fourier transform of (b). (f) Fourier transform of (c). The yellow, red and green lines correspond to the double wedge boundaries of points $\boldsymbol{x}_1$, $\boldsymbol{x}_2$ and $\boldsymbol{x}_3$, respectively.

well, which demonstrates that the image quality strongly depends on the shape and location of the structure to be reconstructed. It indicates that in medical applications, clinically important information may be obscured completely.

The SVDL model is based on the local Fourier transform. The Fourier transform of the top circular area (Fig. 2(b)) and the double wedge boundaries of its center point $\boldsymbol{x}_1$ is shown in Fig. 2(e). The Fourier transform of the top (Fig. 2(c)) or bottom line is shown in Fig. 2(f), and the double wedge boundaries of their center points $\boldsymbol{x}_2$ and $\boldsymbol{x}_3$ are shown in red and green lines. Though some frequency components are lost inside the double wedges for the top circle and the bottom line, the major frequency components are available. For the left and right vertical line structures, their frequency components are almost in the horizontal direction and more information is available. Therefore, they can be reconstructed very well. However, the line at the top position loses the major frequency components and the wTV algorithm is not able to reconstruct it.

3.2 Size Dependency

Fig. 3 shows that wTV can reconstruct the shorter rectangles very well while it fails to recover the upper part of the longer rectangles. We can take the points $\boldsymbol{x}_4$ and $\boldsymbol{x}_5$, which are the centers of top 6th and 16th rectangles, to analyze the data loss double wedges drawn in black and red lines, respectively. Comparing Fig. 3(b) with Fig. 3(a), with increasing length the principal frequency components are more focused around the 0° direction and less measured data are available outside the double wedge area. Therefore, it becomes much harder to reconstruct. As the black double wedges are narrower than the red ones, which means that at lower parts of the phantom more frequency components are available, the lower part can be reconstructed well even in the case of 150×5 phantom.

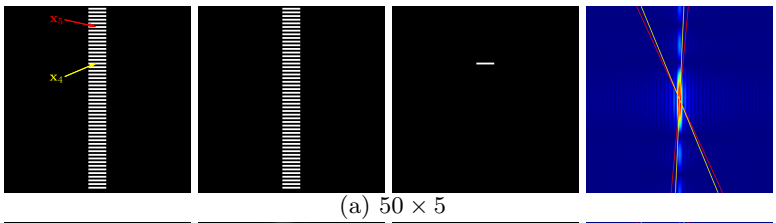

(a) 50×5

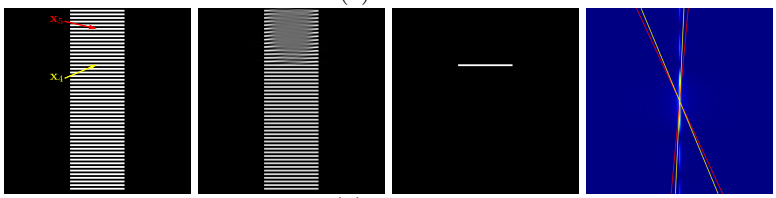

(b) 150×5

Fig. 3. Results for the second group of phantoms. From left to right: phantom, reconstruction, top 16th rectangle, Fourier transform of the 16th rectangle. The yellow and red lines correspond to the data loss double wedge boundaries of points $\boldsymbol{x}_4$ and $\boldsymbol{x}_5$.

3.3 Orientation Dependency

Fig. 4(a) shows that wTV can reconstruct all the rectangles very well in the scan trajectory $(\beta_{\min}, \beta_{\max}) = (-10°, 150°)$ while it fails to reconstruct most rectangles in the trajectory $(\beta_{\min}, \beta_{\max}) = (10°, 170°)$. We take the center points at the top 6th and bottom 10th rectangles, $\boldsymbol{x_6}$ and $\boldsymbol{x_7}$, to analyze the data loss double wedge in different scan trajectories. Fig. 4(f) shows that in trajectory $(\beta_{\min}, \beta_{\max}) = (-10°, 150°)$ most frequency components are outside both the red and green double wedges, therefore all the rectangles can be reconstructed very well. Fig. 4(g) shows that most frequency components are inside the red double wedge but outside the green double wedge in trajectory $(\beta_{\min}, \beta_{\max}) = (0°, 160°)$, that is why wTV can reconstruct most lower rectangles but fails at the area around point $\boldsymbol{x_6}$. Fig. 4(h) shows that more frequency components are inside the red and green double wedges in trajectory $(\beta_{\min}, \beta_{\max}) = (10°, 170°)$ and thus most rectangles are blurred. However, since the green double wedge is much narrower, the very bottom rectangles are still recovered.

4 Discussion

Based on the above experiments, we can conclude that the reconstructed image quality depends on the relationship of source trajectory and geometric structure of the imaged object, position, shape, size and orientation in particular. Fundamentally, whether the wTV algorithm or any type of reconstruction method can reconstruct the object structure depends on the quantity of acquired data according to the shift-variant data loss model.

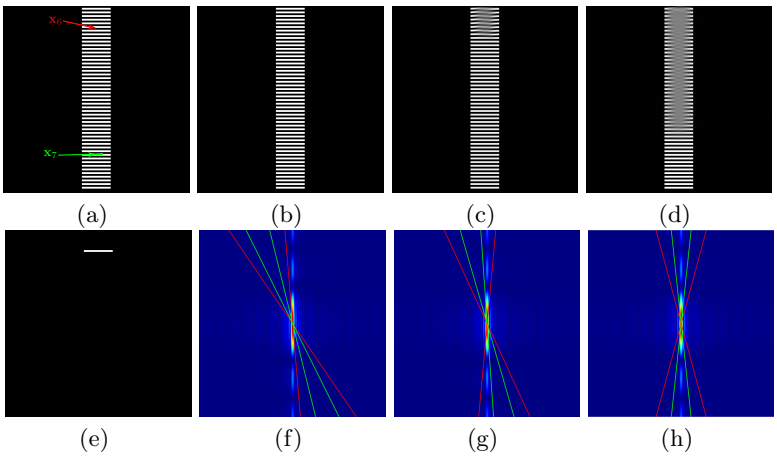

Fig. 4. (a) Phantom. (b) Reconstruction, $(\beta_{\min}, \beta_{\max}) = (-10°, 150°)$. (c) Reconstruction, $(\beta_{\min}, \beta_{\max}) = (0°, 160°)$. (d) Reconstruction, $(\beta_{\min}, \beta_{\max}) = (10°, 170°)$. (e) 6th rectangle in the phantom. (f), (g) and (h) are Fourier transforms of (e). The red and green lines in (f), (g) and (h) correspond to the double wedge boundaries at points $\boldsymbol{x}_6$ and $\boldsymbol{x}_7$ in different trajectories as (b), (c) and (d), respectively.

Disclaimer : The concepts and information presented in this paper are based on research and are not commercially available.

References

1. Bartolac S, Clackdoyle R, Noo F, Siewerdsen J, Moseley D, Jaffray D. A local shift-variant Fourier model and experimental validation of circular cone-beam computed tomography artifacts. Med Phys. 2009;36(2):500–512.
2. Ritschl L, Bergner F, Fleischmann C, Kachelriess M. Improved total variation-based CT image reconstruction applied to clinical data. Phys Med Biol. 2011;56(6):1545–1561.
3. Sidky EY, Pan X. Image reconstruction in circular cone-beam computed tomography by constrained, total-variation minimization. Med Phys. 2008;53(17):4777–4807.
4. Chen Z, Jin X, Li L, Wang G. A limited-angle CT reconstruction method based on anisotropic TV minimization. Phys Med Biol. 2013;58(7):2119–2141.
5. Wu H, Maier A, Fahrig R, Hornegger J. Spatial-temporal Total Variation Regularization (STTVR) for 4D-CT Reconstruction. 2012;8313.
6. Sidky EY, Kao CM, Pan X. Accurate image reconstruction from few-views and limited-angle data in divergent-beam CT. J Xray Sci Technol. 2006;14:119–139.
7. Candès EJ, Wakin MB, Boyd SP. Enhangcing Sparsity by Reweighted l_1 Minimization. J Fourier Anal Appl. 2008;14:877–905.
8. Maier A, Hofmann H, Berger M, Fischer P, Schwemmer C, Wu H, et al. CONRAD - A software framework for cone-beam imaging in radiology. Med Phys. 2013;40(11):111914.